https://doi.org/10.5194/egusphere-2026-2797
Preprint. Discussion started: 14 July 2026

Passive seismic tomography of a gas emitting structure: the case of Nirano Mud Volcanoes (Northern Italy)

Nicolò Carfagna[1], Albachiara Brindisi[1], Dario Albarello[1]

[1] Department of Physical, Earth and Environmental Sciences, University of Siena, Italy

Correspondence to: Nicolò Carfagna (nicolo.carfagna@student.unisi.it)

Abstract. In this work, Ambient Noise Tomography (ANT) is applied for a 3D subsurface reconstruction in terms of shear-wave velocity (Vs) beneath one of the main emissive vents of the Nirano Mud Volcanoes site (northern Italy). The adopted workflow is based on short ambient noise records (~1h) acquired with a small seismic array composed of vertical geophones and implements an automated procedure to capture seismic heterogeneities in the subsoil volume. This procedure can be of general interest when the use of more invasive procedures is hampered by the logistic or economic limitations. In the case here considered a low shear-wave velocity anomaly is identified right below the emissive vent extending vertically from the surface up to approximately 30 m depth. A quantitative model is proposed to explain the correspondence of the low velocity anomaly and emitting vents in terms of increased porosity and saturation of hosting sediments, where deep seated fluids and gas may accumulate close to the surface. This may increase the possible hazard relative to potentially damaging eruptions in the case of a sudden release of the gas stored in this shallow reservoir.

1. Introduction

In volcanic and geothermal environments, the near-surface structure plays a fundamental role in the final steps of migration and accumulation processes of fluids and gases that then reach the surface. Surface deposit geometries and their physical properties are therefore crucial in the interpretation of subsurface volcanic and hydrothermal processes and in monitoring temporal changes in active systems, in the assessment of the associated risks and their potential impact on local populations and infrastructure. In this context, seismic methods represent a powerful tool for this type of investigation, as they provide quantitative and generally non-invasive characterization of the subsurface mechanical properties in such complex contexts (e.g., Chouet, 2003). Among the seismic methods, the ambient noise-based approaches have become an interesting and advantageous alternative compared to common active methods, particularly in protected sites or complex contexts where the use of controlled sources can be impractical or not allowed, as the case of active volcanic or geothermal sites.

In context of gas emitting structures, seismic wave velocity models, both in terms of Vp and Vs, represent highly useful parameters for characterizing the subsurface configuration of shallow or deeper reservoirs in terms of fluid saturation and porosity (e.g., Lee 2004; Tsai et al. 2023; Tsai and Asimaki 2026).

Among these contexts, Mud Volcanoes (MV hereafter) represent a case of great scientific and environmental interest. MV are geological structures distributed in both continental and offshore contexts, associated with the surface outflow of deep

https://doi.org/10.5194/egusphere-2026-2797
Preprint. Discussion started: 14 July 2026

fluids, mud and gases (particularly CH4 and CO2) with relevant implications for the atmospheric greenhouse gas balance, geological hazard and the exploration of energy resources (Mazzini & Etiope, 2017). The characterization of the subsurface feed processes of these systems, however, is complex, as emissions are rarely concentrated at the main surface vents but distributed over larger areas through articulated networks of ducts and minor paths hard to identify with direct methods. In this context, passive seismic imaging methods, in particular Ambient Noise Tomography (ANT), represent a promising tool to provide high-resolution characterization of the structure and dynamics of the subsurface close to the emissive vents (e.g., Brenguier et al., 2007), even where marked lateral variations in the physical properties are expected at the scale of few tens of meters.

Moreover, the Nirano site is also a touristic attraction visited by hundreds of citizens per year. Since in some cases potentially dangerous paroxystic activity of mud volcanoes may occur (e.g., Bonini, 2009), as tragically demonstrated during the Maccalube eruption in Southern Italy responsible for victims among the visitors (AGI, 2014), a more detailed knowledge of potential shallow depth secondary reservoirs may be of help for risk assessment.

This work proposes the application of a surface-wave tomographic approach based on ambient seismic noise for the 3D reconstruction of the subsurface in terms of Vs beneath one of the main emissive vents of the Nirano site, where previous studies have already provided insights into the subsurface structure through common seismic approaches (Antunes et al., 2022; Brindisi et al., 2023; Carfagna et al., 2024). The adopted workflow is based on short records (~1h) acquired with a small-scale array. Inter-station phase dispersion curves are extracted for all pairs of sensors, and a linear tomographic inversion scheme is used to retrieve phase velocity maps within the investigated frequency range. Finally, a rapid 1D local dispersion curve inversion is adopted in order to obtain a Vs 3D model below the investigated domain. Each step of the workflow is largely automated, making the entire procedure computationally efficient.

The resulting Vs model is then interpreted in the context of the site fluid and gas dynamics, also integrating seismic observations available in the literature for the area (Accaino et al., 2007; Antunes et al., 2022; Brindisi et al., 2025) in order to characterize the shallow feed system and to provide an estimate of the physical properties of the sediment inside and outside the observed anomaly.

2. Geological Setting

The 'Salse di Nirano' (Fig. 1) represents one of the best-known mud volcanism sites in Italy, classified as a Nature Reserve since 1982 (Martinelli & Judd, 2004). The site is located within the Apennine thrust belt, overlying a Pliopleistocene marine clay formation ("Argille Azzurre") locally interrupted by buried faults acting as preferential paths connecting the surface to a deep reservoir of both fluid and gases (Bonini, 2008; 2009). The area hosts four modest-sized volcanic vents aligned in the ENE-WSW direction with heights up to about 3 m, accompanied by numerous smaller conduits distributed across the entire area with emissive activities varying in both time and space. Geochemical investigations (Sciarra et al., 2019) indicated that the outgassing process is not concentrated at the main cones, but it is distributed over a larger area elongated in the same

https://doi.org/10.5194/egusphere-2026-2797
Preprint. Discussion started: 14 July 2026

direction of the main vents (ENE-WSW), with the northeastern sector recently identified as the most active in terms of concentration and gas flow. The main gases emitted are CH_4 and CO_2, with average measured fluxes around 221 mg m^{-2} d^{-1} and 18 g m^{-2} d^{-1}, respectively, corresponding to an overall mean volumetric flux of the order of 9.0×10^{-3} m^3 d^{-1} m^{-2} (Sciarra et al., 2019). Similar value of the gas outflow was also estimated by seismic methods in the assumption that the seismic signals produced by the volcanic activity correspond to gas bubble burst all beneath the site (Carfagna et al., 2024).

Geophysical prospecting (Accaino et al., 2007; Oppo, 2011; Lupi et al., 2016; Giambastiani et al., 2022; Nespoli et al., 2023) indicates that significant lateral heterogeneities exist in the seismic configuration of the shallow subsoil (10-20 m of depth) where deep fluids are temporarily trapped before reaching the surface. Both active and passive seismic prospecting (Antunes et al., 2022; Brindisi et al., 2023; Carfagna et al., 2024) were conducted within the area to constrain the seismic structure of the shallow subsoil, revealing marked velocity variations even at the scale of few tens of meters.

Within the emitting area, Vp values increase from few hundreds m/s close to the surface (<3 m) up to 1500-2000 m/s in the deeper bedrock. Vs values increase from about 100 m/s in the first 3 m layer and gradually increase to about 400 m/s below 30 m. Close to the main vents, a potentially low velocity zone is locally detected within 2 and 10 m of depth which may suggest a local accumulation of mud and brines. To provide a more detailed 3D reconstruction of these possible reservoirs close to the surface a passive seismic campaign was planned by focusing on the vent closer to the visitors access road (Fig. 1).

3. Experimental setting and data processing

3.1 Data acquisition

The acquisition of seismic ambient noise data was conducted in October 2025 using a seismic array (Fig. 1) composed of vertical geophones with a natural frequency of 4.5 Hz, connected to a BrainSpy™ digital acquisition system, produced by Moho s.r.l. The array (blue triangles in Fig. 1), with geometry specifically designed to allow subsequent 2D tomographic inversion, consisted of two parallel branches, each composed of eight geophones each. An inter-station distance of 5 m between the geophones was chosen along the two branches, while the distance between the two branches was set at 40 m. The array was placed in the eastern part of the site, just above one of the main emission cones and therefore the most recently active zone. The overall recording duration for both arrays was approximately 1 hour with the same sampling rate (256 sps), ensuring in all cases enough data for subsequent dispersion analyses.

https://doi.org/10.5194/egusphere-2026-2797
Preprint. Discussion started: 14 July 2026

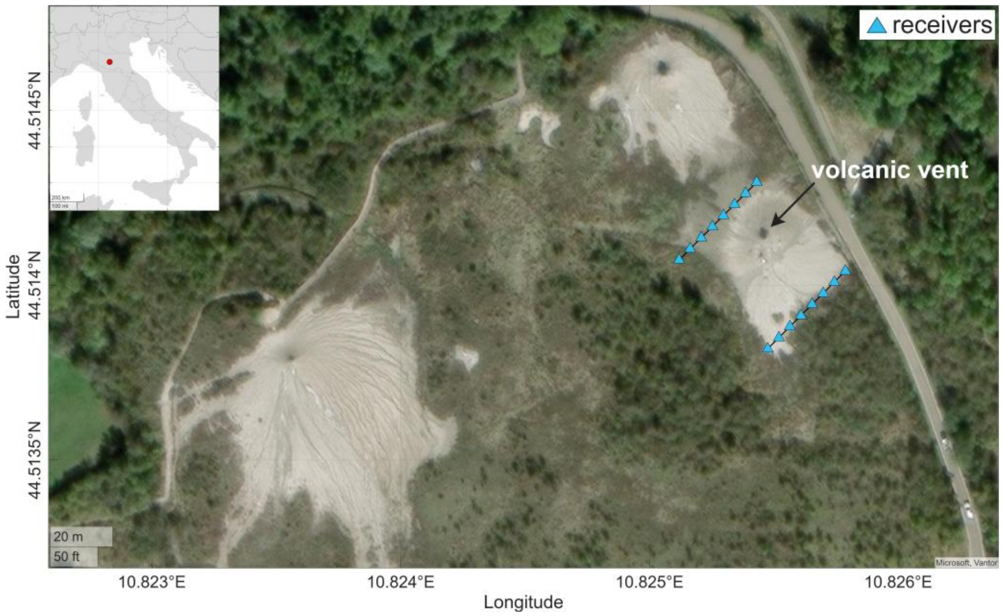

Figure 1 - Satellite image of the study area and experimental setup of the deployed seismic instruments. The blue triangles indicate the positions of the 16 vertical geophones arranged in two parallel branches with an inter-station distance of 5 m and 40 m between the two branches. The black arrow indicates the emissive point below which the array has been arranged. Background satellite imagery © Microsoft, Vantor. The map was created using ArcGIS® Pro software by Esri | Powered by Esri.

3.2. Rayleigh dispersion curve retrieval

The ambient noise record was processed to achieve Rayleigh phase dispersions curve for each inter-station path within the array. Inter-station phase dispersion curves are estimated through common two-station approaches (e.g., Ekström et al., 2009; Magrini et al., 2020) based on standard spectral analysis (Aki, 1957; 1965). The time traces are first divided into set of overlapping time windows, then, for each pair of simultaneous windows, the normalized cross-spectrum (or coherency) is computed in the frequency-domain (see Malagnini et al., 1993; Ohori et al., 2002; Parolai et al., 2006) and stacked to achieve the azimuthal average Spatial Autocorrelation function (or SPAC function). The SPAC function is modelled as zero-th Bessel function, and a grid search procedure is adopted to identify phase velocities compatible with observations. Eventual non-uniqueness problems experimental group velocity dispersion curves (Dziewonski et al., 1969) were also computed and compared with the one expected from each possible phase velocity dispersion curve. The best-fitting synthetic group curve is taken as the one corresponding to the correct phase dispersion curve which has been automatically selected. At the end of the phase curve selection, 94 inter-station curves were automatically obtained, and about 70 out of these were considered suitable for the following analysis.

https://doi.org/10.5194/egusphere-2026-2797
Preprint. Discussion started: 14 July 2026

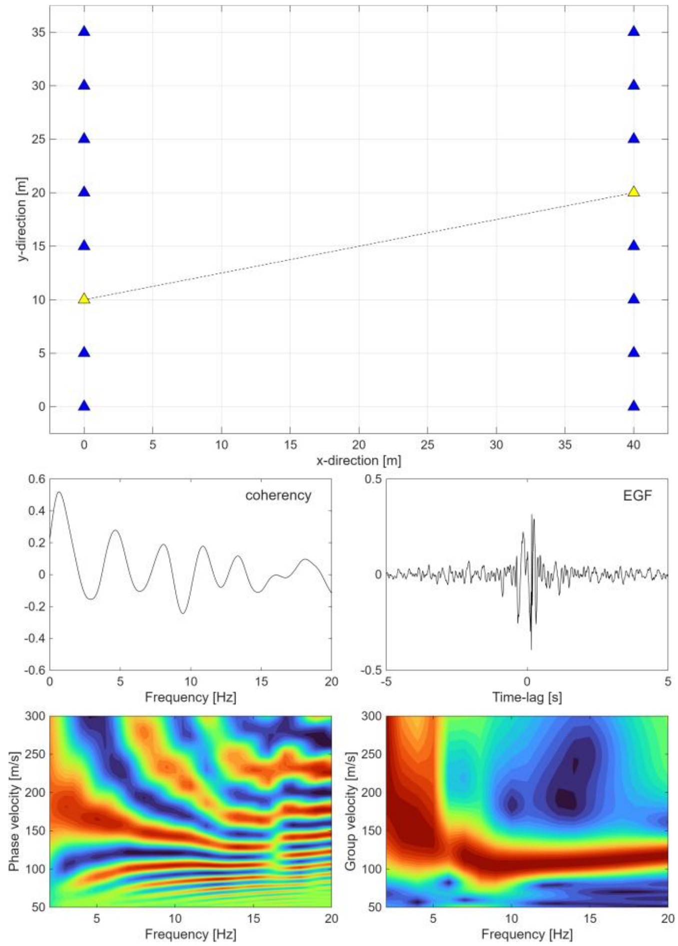

Figure 2 - Schematic example of the results of two-station dispersion analysis. The upper panel shows the arrangement of the receivers along two parallel branches and the pair of stations used for the analysis (yellow triangles). The middle panels show, respectively, the frequency-domain normalized cross-spectrum and the time-domain EGF obtained by correlating the signals recorded by the two sensors. The lower panels show the obtained frequency-velocity (phase and group) spectra, which are then joint used in the automatic picking procedure.

3.3. Rayleigh-wave phase velocity maps

Based on the selected dispersion curves, travel time values were obtained for each frequency and station-station path. In common approaches, the observed travel-times are inverted for each sampled frequency separately in order to obtain a set of phase velocity maps at discrete frequencies. Here instead the linear tomographic inversion is applied as one-step strategy (no iterations are implemented) considering all frequencies simultaneously (Mohammadi et al., 2020). The linear inverse problem is solved through a damped and weighted least-square solution (Menke, 2012; Fichtner, 2021) for which damping (or regularization) parameters are applied both over the space and the frequency for adjacent model parameters. The use of two different damping parameters allows to suppress abrupt variations of the final model both in space and along the considered frequency range, thus remaining constrained to the smooth nature of the dispersion curves.

https://doi.org/10.5194/egusphere-2026-2797
Preprint. Discussion started: 14 July 2026

Given the extent of the 2D investigated domain (40x35m), multiple trial cell sizes were tested to optimize spatial discretization. A square cell size of 2.5m has been finally adopted, corresponding to 224 model parameters for each frequency. For tomographic inversion, discrete frequencies with a step size of 1 Hz in the range 2–36 Hz were considered, for a total of 224 × 35 parameters within the one-step inversion. The number of travel-times varies with frequency, from a maximum around 90 observations (e.g., in the 5–20 Hz range) up to a minimum of about 60 at extreme frequencies. The best performing solution was chosen to account for the overall root-mean-square residuals (RMSr) for all considered frequencies and through a compromise between model resolution and inversion stability. Moreover, solutions obtained combining different set of regularization parameters were also considered and pretty much the same overall results were obtained, considering the main structures highlighted from the data.

A set of obtained phase velocity maps is shown in Fig. 3, also reporting the associated RMSr after the adopted inversion scheme. Considering the RMSr calculated over the entire frequency range, its value generally remains low with the average RMSr, considering all frequencies, that is approximately 0.005s. At lower frequency (2–3 Hz) the RMSr reaches values around 0.009s; for all other frequencies it is lower, with minimum values of around 0.0012s in the intermediate frequency range between around 10 Hz and 30 Hz. At all considered frequencies the residual distributions associated with the observed station-station paths show an overall average close to 0, indicating the absence of strong biases on the observed data, and residual standard deviations typically on the order of 10^{-4} s.

https://doi.org/10.5194/egusphere-2026-2797
Preprint. Discussion started: 14 July 2026

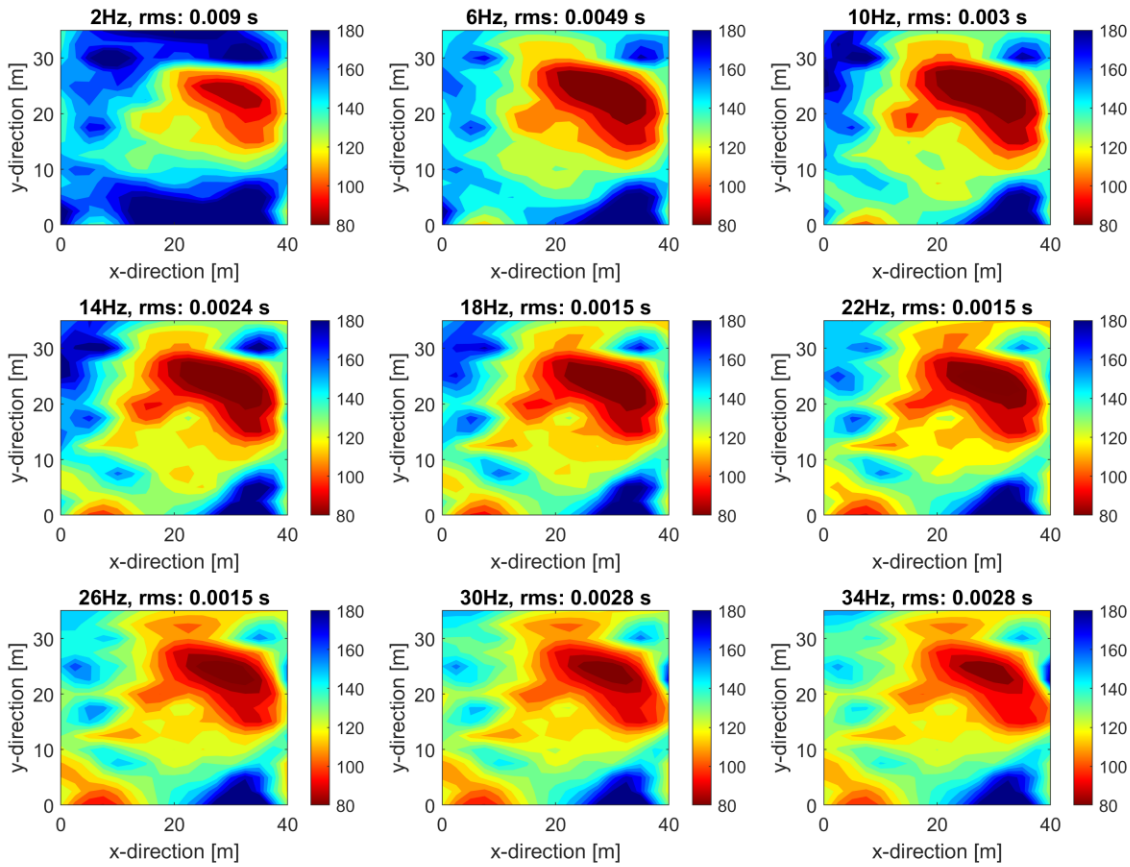

Figure 3 - Phase velocity maps obtained at nine representative frequencies of the investigated range (from 2 Hz to 34 Hz). The maps highlight the spatial evolution of Rayleigh phase velocities as function of the considered frequency and show patterns that are relatively consistent over the frequency range. For each phase map, the associated root-mean-square residual is also reported.

3.4. Estimate of the Vs profiles

Given the large number of local dispersion curve provided by the travel-time inversion (as many as the 2D model parameters), common explorative methods (e.g., Genetic Algorithm and Neighbourhood Algorithm) used to infer local 1D shear wave velocity profile can be extremely time-consuming.

The approach here adopted is based on iterative forward modelling strategy, without the need for explicit inversions or derivatives computation. Starting from an initial guess model, shear wave velocities associated with discrete layers are progressively updated while keeping the number and thickness of the layers fixed and a constant Vp/Vs ratio over the entire velocity model.

The initial model (Vp, Vs and ρ) is directly retrieved from the observed dispersion curve $V_R(f)$ based on the simple assumption that surface waves depth penetration increases as the considered frequency decreases ($\lambda = V_R/f$), and that depth penetration and relevant wavelength take the same order of magnitude (Jones, 1958; 1962). Assuming Rayleigh phase

https://doi.org/10.5194/egusphere-2026-2797
Preprint. Discussion started: 14 July 2026

velocities at a given frequency as a fraction of the shear wave velocities up to that depth (e.g., $V_S \approx V_R/0.9$) a first estimate of $\langle Vs \rangle_z$, i.e. the average V_S up to the considered depth z (e.g., Socco et al., 2017; Socco & Comina, 2017). The average V_S profile can be then discretized into a stack of homogeneous layers, each one with its own Vs_i value, while Vp_i values are finally computed from the Vs_i through a fixed Poisson ratio (ν) and density values (ρ) are also kept constant along the stratified model.

Starting from this initial model and the corresponding solution in terms of phase dispersion curve, a misfit value in the form of root-mean-square of percentual difference between observed and modelled curves is evaluated. The sign of the residual at frequency f_i, considering the adopted frequency–layer relationship, guides the Vs_i updates direction consistently with the residual value. To account for the fact that Rayleigh waves do not focus at a single depth but, in contrast, are distributed over a wider vertical range, the residual associated with each frequency is vertically weighted in the model through a sensitivity kernel of Rayleigh phase velocities numerically computed only once for the initial model.

Of the 224 obtained local dispersion curves, approximately 80% were reproduced satisfactorily (all residuals distributed in frequency less than 1% of the percentual difference), while in the remaining 20% of curves, the total RMS still fell within 8% of the overall gap, confirming the ability to provide effective solutions with a very low computational cost.

As a validation, one of the local dispersion curves was inverted adopting both Genetic Algorithms (GA; Goldberg, 1989) and the proposed approach, considering different combinations of initial parameters (Poisson ratio, wavelength-depth scale factor, number and thickness of the layers). Fig. 4 shows the Vs profiles obtained with the proposed method falling within the range of solutions identified by multiple runs of GA, confirming that the information directly derived from the observed dispersion curve is sufficient to provide an effective initial estimate of the subsurface structure, even in the lack of prior constraints.

https://doi.org/10.5194/egusphere-2026-2797
Preprint. Discussion started: 14 July 2026

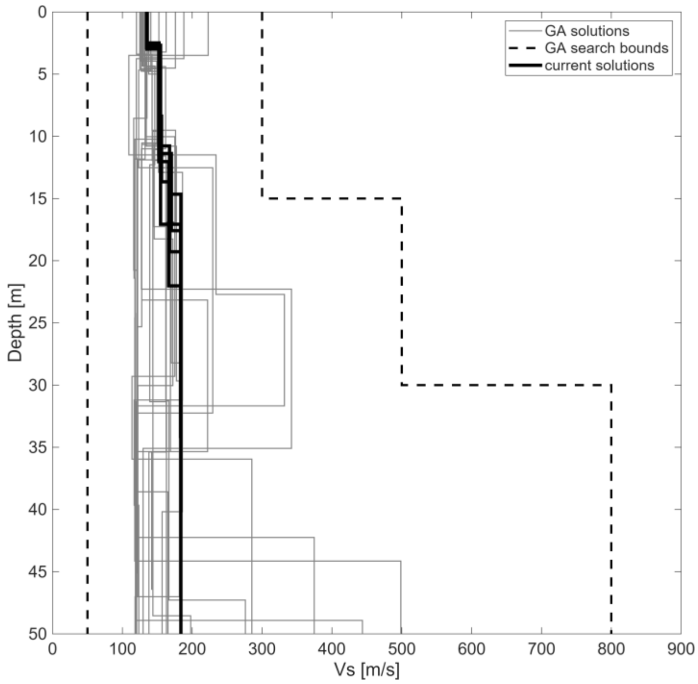

Figure 4 - Comparison between shear wave velocity models obtained by genetic algorithm (GA) inversion and the models derived from the proposed approach. The grey profiles represent the set of models obtained from the different GA inversions, while the black profiles are the model estimated through the current method using different combination of initial parameters (z_{coef} and Poisson ratio) and different number and thickness of the model layers. The black dashed lines represent the range of parameters explored during the GA search. The comparison shows that the model obtained with the proposed method falls within the range of compatible solutions identified by multiple GA inversions.

4. Vs model interpretation

In Fig. 5 the obtained shear wave velocity model is illustrated as a set of horizontal Vs slices at different depths. The model highlights the presence of a well-defined low-velocity structure located approximately beneath the emissive vent, which progressively extends towards the surface, while at depth it appears laterally confined. The minimum Vs values, less than 100 m/s, are concentrated between approximately 5 and 10 m depth.

Compared to the phase velocity maps (Fig. 3), low-velocity anomaly appears slightly more extended than initially suggested, while its dimensions reduce at depth. Furthermore, at greater depths (30 m slice in Fig. 5), the low-velocity area appears to be laterally well confined in one direction by higher-velocity materials, while in the other direction it appears to extend beyond the investigated domain, towards the adjacent volcanic cone with respect to the one under investigation. Overall, the low-velocity structure represents a coherent feature, consistent with the vent's feeding system. The geometry of the observed low velocity zone is also compatible with independent P-waves seismic tomography model obtained at another vent in the same area (Accaino et al., 2007). A more detailed inspection of the inverted Vs profiles from the model (Fig. 6) shows that

https://doi.org/10.5194/egusphere-2026-2797
Preprint. Discussion started: 14 July 2026

deeper the profiles clearly separate into two distinct groups: profiles inside the anomaly (solid grey) take the lowest Vs values that never exceed 150 m/s, while the Vs profiles at the edges of the domain (dashed black) reach values of 240 m/s, confirming the well-defined confinement of the anomaly at depth.

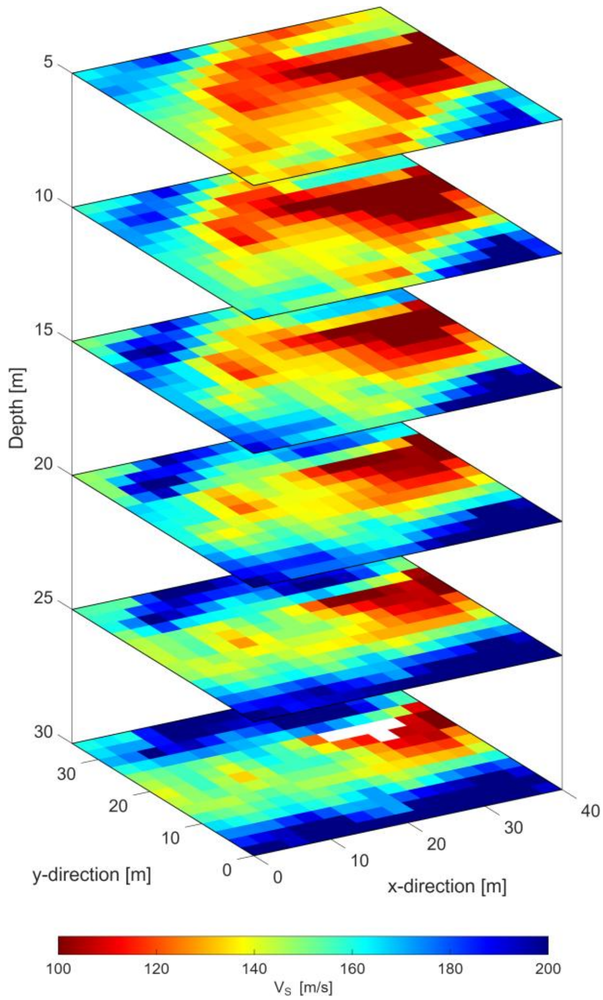

Figure 5 - Plot of the shear wave velocity (Vs) model obtained. The model is represented by a set Vs maps at depths 5 m 10 m, 15 m, 20 m, 25 m and 30 m, which allow to visualize the geometry of the main structure and its vertical and lateral variability within the studied volume.

https://doi.org/10.5194/egusphere-2026-2797
Preprint. Discussion started: 14 July 2026

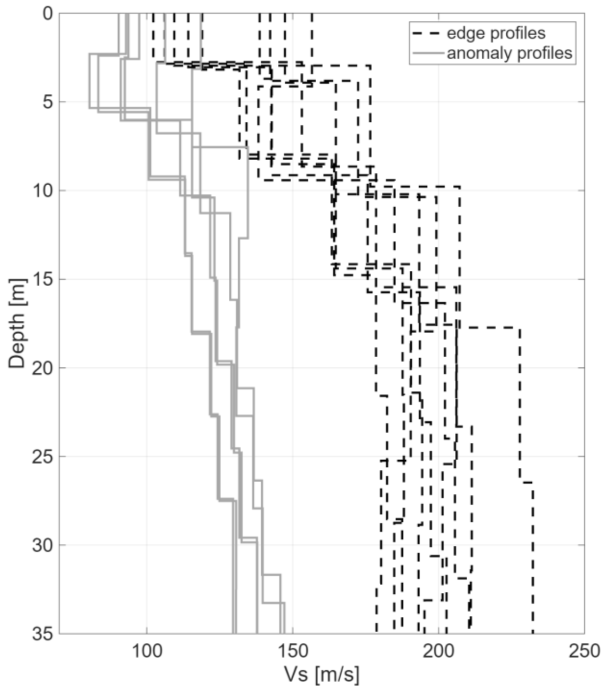

Figure 6 - Selected Vs profiles extracted from the 3D model. Dashed black profiles refer to the edges of the investigated domain, outside the low-velocity anomaly, while continuous grey profiles refer to Vs values within the anomaly. In the shallowest portion of the model the differences between the two groups are less marked, with the profiles progressively separating at depth and remaining quite different below 10 m, where the profiles inside the anomaly maintain Vs values strictly below 150 m/s while the external ones reach values around 240 m/s.

Unlike Accaino et al. (2007), who identified a mud chamber (Vp ~1100 m/s) within the deeper bedrock (Vp ~1700-2300 m/s) beneath the most western vent in the area, the S-wave tomography presented in this work highlights with higher resolution the uppermost part of the feed system, revealing a vertical low-velocity structure (Vs ~80-90 m/s) within the softer shallow deposits down to 30 m depth, interpretable as a preferential fluid upwelling conduit. Notably, the relative velocity contrast inside and outside the anomaly is of the same order of magnitude in the two studies.

By integrating the Vs values obtained from the present study with the Vp values available in the literature for the NMV area (e.g., Antunes et al., 2022; Brindisi et al., 2025), a simplified two-layer model of the subsurface can be proposed: a shallow softer deposit, consisting of emission mud and weathered clays, characterized by Vs of 180-200 m/s and Vp of about 450-550 m/s, and a deeper and more rigid Pliopleistocene clay bedrock (Argille Azzurre formation), with Vp of the order of 1700-2300 m/s. Within the shallow deposit, a low-velocity conduit (Vs ~80-90 m/s) extends essentially vertically up to about 30 m depth, while Accaino et al. (2007) identified a mud chamber characterized by Vp of about 1100 m/s within the deeper bedrock. These two elements, i.e. the surface duct and the deeper mud chamber, which have been found beneath different volcanic vents, can be interpreted as parts of the same near-surface emissive system.

https://doi.org/10.5194/egusphere-2026-2797
Preprint. Discussion started: 14 July 2026

In order to provide a more detailed interpretation of the observed anomaly, an attempt was made to estimate the physical properties of the sediment inside and outside the anomaly highlighted in this study following Lee (2004) based on the modified Biot-Gassmann theory (BGTL). Starting from the observed reduction of Vp in the mud chamber (Vp_{in}), similar effect was hypothesized also in the softer deposits investigated in the present study. By applying at the shallow layer (Vp ~ 500 m/s outside the anomaly, Vp_{out}) the same Vp reduction factor an estimated Vp value within the anomaly of approximately 270 m/s is obtained. Combining the estimated Vp with the Vs from the 3D model (80-90 m/s inside the anomaly and 180-200 m/s outside), the BGTL model suggests the water saturation remains substantially unchanged inside and outside the anomaly, whereas porosity increases significantly, from 12% in the surrounding material to approximately 21% inside the duct. Given the uncertainty associated with the considered Vp values and the reduction factor inferred from Accaino et al. (2007), a sensitivity analysis was conducted by varying Vp from -25% to +25% of the reference value and considering different ratios between Vp inside and outside the anomaly. The results show that, regardless of the assumed Vp, porosity inside the anomaly is systematically higher than in the surrounding material (0.22–0.31 inside, 0.1–0.17 outside), supporting the proposed interpretation. Water saturation, on the other hand, exhibits larger variability and should therefore be interpreted more cautiously. Nevertheless, both inside and outside the anomaly, water saturation varies proportionally with porosity. Another important aspect to highlight is that Vp generally increases with increasing water saturation, whereas lower Vp values are associated with lower water and higher gas saturation.

The increase in porosity also explains the observed Vs decrease, which does not appear to be directly related to changes in gas content, but rather to zones of weaker sedimentary matrix characterized by higher porosity beneath the main volcanic vents. The higher porosity observed within the anomaly has direct implications for the local permeability and, consequently, for the fluids flow feeding the surface mud volcano's activity. The relationship between porosity and permeability is far from straightforward, as permeability depends not only on porosity itself, but also on pore connectivity (open or closed porosity) and on the specific surface area between pores and the solid matrix (Sibiryakov et al., 2021). In this view, a medium may exhibit high total porosity while still maintaining very low permeability if the pores are predominantly isolated. However, in general terms, an increase in porosity is expected to enhance permeability, especially in the case of open porosity, where permeability may increase much more strongly because of the nonlinear relationship between the two variables (e.g., Zheng et al., 2015). The observed surface emissive activity (rising gas and liquid mud) indicates that the porous network beneath the vent is effectively percolating. The physical properties of the shallow portion of the medium can therefore play a fundamental role in controlling accumulation and migration of fluids towards the surface. Where permeability is insufficient to make a continuous outflow, gas can accumulate under pressure in the subsurface, increasing the risk of sudden and potentially violent release.

Indeed, although widespread outgassing processes are documented across the entire area hosting the four volcanic vents (Sciarra et al., 2019), reflecting the high gas content in the shallow subsoil, concentrated mud emissions are restricted to the main emissive cones and to small nearby pools. This discrepancy suggests that the localized increase in porosity and permeability beneath the vents creates optimal conditions for a more intense and continuous upward migration of gas,

https://doi.org/10.5194/egusphere-2026-2797
Preprint. Discussion started: 14 July 2026

capable of dragging fine-grained sediments into suspension and producing the surface emission of liquid mud. Moreover, changes in pore geometry within the anomaly cannot be excluded. Larger and more regularly shaped pores may reduce the specific surface area of the pore network, leading to a further increase in permeability. These mechanisms are not mutually exclusive and may jointly contribute to the low-velocity anomaly identified by tomography.

5. Conclusion

The joint use of surface wave tomography from short ambient noise records with the rapid local inversion of the dispersion curves allowed us to obtain a 3D Vs model beneath one of the main emissive vents within the NMV area. The Vs model, as well as the Rayleigh phase velocity maps, reveals the presence of a geometrically well-defined low-velocity anomaly, extending from the surface to about 30 m depth and which might be interpreted as a fluid upwelling conduit, given the observed surface gas and fluid seepage. This structure is also clear in the phase velocity maps before the 1D inversion, confirming the reliability of the observed feature.

By integrating the obtained Vs model with Vp values available in literature for the studied area and applying the modified Biot-Gassmann theory, the observed Vs velocity anomaly is mainly attributed to an increase in porosity in the ascent area (beneath the vent), from about 12% on the outside to about 21% on the inside, rather than to a direct effect of gas content which has greater effect on Vp. This increase in porosity, potentially accompanied by variations in pore geometry, is compatible with an increase in permeability (open porosity) that would favour the preferential upward migration of fluids and gases observed at the surface. The results further suggest that the diffuse outgassing observed over the entire area reflects the high gas content in the surface deposits, while the concentrated mud and gas emission in the main cones is controlled by the localized increase in porosity and permeability that characterizes the near-surface structure beneath the volcanic vents. These findings can also have direct implications in the evaluation of the local hazard, since shallow gas reservoirs might represent a potential source of paroxystic activity right beneath the surface.

Code and data availability

All the codes developed and used in this study, including those for inter-station dispersion curves extraction, travel-time tomographic inversion of Rayleigh phase velocities, and local inversion of dispersion curves for the estimation of 1D Vs profiles, are available upon request to the corresponding author (N. Carfagna; nicolo.carfagna@student.unisi.it).

https://doi.org/10.5194/egusphere-2026-2797
Preprint. Discussion started: 14 July 2026

Author contributions

N. Carfagna: Conceptualization, Methodology, Software, Formal analysis, Investigation, Writing – original draft. **A. Brindisi**: Writing – review & editing, Investigation, Validation, Formal analysis. **D. Albarello**: Conceptualization, Formal analysis, Resources, Writing – review & editing, Funding acquisition.

Competing interests

The authors state that they have no known competing financial interests, personal relationships, or conflicts of interest that might have appeared to influence the work reported in this article.

References

Accaino, F., Bratus, A., Conti, S., Fontana, D., & Tinivella, U.: Fluid seepage in mud volcanoes of the northern Apennines: An integrated geophysical and geological study. *Journal of Applied Geophysics*, *63*(2), 90–101. https://doi.org/10.1016/j.jappgeo.2007.06.002, 2007

AGI (Agenzia Giornalistica Italia): Small volcano erupts in Sicily killing two children. Available at: https://www.agi.it/archivio/storico/news/2014-09-27/small_volcano_erupts_in_sicily_killing_two_children-15620/, [Accessed: 15 May 2026], 2014

Aki, K.: Space and Time Spectra of Stationary Stochastic Waves, with Special Reference to Microtremors. *Bullettin of Earthquake Research Institute*, *35*, 415–457, 1957

Aki, K.: A note on the use of microseisms in determining the shallow structure of the Earth's crust. *Geophysics*, *30*(4), 665–666. https://doi.org/10.1190/1.1439640, 1965

Antunes, V., Planès, T., Obermann, A., Panzera, F., D'Amico, S., Mazzini, A., Sciarra, A., Ricci, T., & Lupi, M.: Insights into the dynamics of the Nirano Mud Volcano through seismic characterization of drumbeat signals and V/H analysis. *Journal of Volcanology and Geothermal Research*, *431*. https://doi.org/10.1016/j.jvolgeores.2022.107619, 2022

Biot, M.: Theory of propagation of elastic waves in a fluid-saturated porous solid. *Journal of Acoustical Society of America*, 28, 2, 168-178, 1956

Bonini, M.: Elliptical mud volcano caldera as stress indicator in an active compressional setting (Nirano, Pede-Apennine margin, northern Italy). *Geology*, *36*(2), 131–134. https://doi.org/10.1130/G24158A.1, 2008

Bonini, M.: Mud volcano eruptions and earthquakes in the Northern Apennines and Sicily, Italy. *Tectonophysics*, *474*(3–4), 723–735. https://doi.org/10.1016/j.tecto.2009.05.018, 2009

Brenguier, F., Shapiro, N. M., Campillo, M., Nercessian, A., & Ferrazzini, V.: 3-D surface wave tomography of the Piton de la Fournaise volcano using seismic noise correlations. *Geophysical Research Letters*, *34*(2). https://doi.org/10.1029/2006GL028586, 2007

Brindisi, A., Carfagna, N., Paolucci, E., Salleolini, M., & Albarello, D.: The fine structure of seismic emissions from the Nirano mud volcanoes (northern Apennines, Italy): a phenomenological study. *Bulletin of Geophysics and Oceanography*, *65*(2), 165–176. https://doi.org/10.4430/bgo00437, 2023

https://doi.org/10.5194/egusphere-2026-2797
Preprint. Discussion started: 14 July 2026

Brindisi, A., Paolucci, E., Carfagna, N., & Albarello, D.: Passive seismic measurements to characterize gas reservoirs in a mud volcano field in Northern Italy. *Marine and Petroleum Geology*, *173*. https://doi.org/10.1016/j.marpetgeo.2024.107275, 2025

Carfagna, N., Brindisi, A., Paolucci, E., & Albarello, D.: Seismic monitoring of gas emissions at mud volcanoes: The case of Nirano (northern Italy). *Journal of Volcanology and Geothermal Research*, *446*. https://doi.org/10.1016/j.jvolgeores.2023.107993, 2024

Chouet, B.: Volcano Seismology. In *Pure appl. Geophys*, 160, 2003

Dziewonski, A., Bloch, S., & Landisman, M.: A technique for the analysis of transient seismic signals. *Bulletin of the Seismological Society of America*, *59*(1), 427–444. https://doi.org/10.1785/BSSA0590010427, 1969

Ekström, G., Abers, G. A., & Webb, S. C.: Determination of surface-wave phase velocities across USArray from noise and Aki's spectral formulation. *Geophysical Research Letters*, *36*(18). https://doi.org/10.1029/2009GL039131, 2009

Fichtner, A.: *Lecture Notes on Inverse Theory*, 2021

Giambastiani, B. M. S., Antonellini, M., Nespoli, M., Bacchetti, M., Calafato, A., Conventi, M., Dadomo, A., Martinelli, G., Morena, M., Venturoli, S., & Piombo, A.: Mud flow dynamics at gas seeps - Nirano Salse, Italy -. *Environmental Earth Sciences*, *81*(19), 480. https://doi.org/10.1007/s12665-022-10615-2, 2022

Goldberg, D. E.: *Genetic Algorithms in Search, Optimization, and Machine Learning*. Addison-Wesley, Reading, Mass, 1989.

Jones, R. B.: In situ measurement of the dynamic properties of soil by vibration methods. *Geotechnique*, *8*(1), 1–21, 1958

Jones, R. B.: Surface wave technique for measuring the elastic properties and thickness of roads: theoretical development. *British Journal of Applied Phyisics*, *13*, 21–29, 1962

Lee, M. W.: Elastic velocities of partially gas-saturated unconsolidated sediments. *Marine and Petroleum Geology*, *21*(6), 641–650. https://doi.org/10.1016/j.marpetgeo.2003.12.004, 2004

Lupi, M., Ricci, B. S., Kenkel, J., Ricci, T., Fuchs, F., Miller, S. A., & Kemna, A.: Subsurface fluid distribution and possible seismic precursory signal at the Salse di Nirano mud volcanic field, Italy. *Geophysical Journal International*, *204*(2), 907–917. https://doi.org/10.1093/gji/ggv454, 2016

Magrini, F., Diaferia, G., Boschi, L., & Cammarano, F.: Arrival-angle effects on two-receiver measurements of phase velocity. *Geophysical Journal International*, *220*(3), 1838–1844. https://doi.org/10.1093/gji/ggz560, 2020

Malagnini, L., Rovelli, A., Hough, S. E., & Seeber, L.: SITE AMPLIFICATION ESTIMATES IN THE GARIGLIANO VALLEY, CENTRAL ITALY, BASED ON DENSE ARRAY MEASUREMENTS OF AMBIENT NOISE. In *Bulletin of the Seismological Society of America*, 83, 6, 1993

Martinelli, G., & Judd, A.: Mud volcanoes of Italy. *Geological Journal*, *39*(1), 49–61. https://doi.org/10.1002/gj.943, 2004

Mazzini, A., & Etiope, G.: Mud volcanism: An updated review. *Earth-Science Reviews*, *168*, 81–112. https://doi.org/10.1016/j.earscirev.2017.03.001, 2017

Menke, W.: Geophysical Data Analysis: Discrete Inverse Theory. In *Geophysical Data Analysis: Discrete Inverse Theory* (Third). Academic Press. https://doi.org/10.1016/b978-0-12-397160-9.00001-1, 2012

Mohammadi, N., Gholami, A., Rahimi, H., & Aoudia, A.: Simultaneous tomography of all periods in surface wave analysis. *Physics of the Earth and Planetary Interiors*, *298*. https://doi.org/10.1016/j.pepi.2019.106338, 2020

https://doi.org/10.5194/egusphere-2026-2797
Preprint. Discussion started: 14 July 2026

Nespoli, M., Antonellini, M., Albarello, D., Lupi, M., Cenni, N., & Piombo, A.: Gravity Data Allow to Image the Shallow-Medium Subsurface Below Mud Volcanoes. *Geophysical Research Letters*, *50*(20). https://doi.org/10.1029/2023GL103505, 2023

Ohori, M., Nobata, A., & Wakamatsu, K.: A Comparison of ESAC and FK Methods of Estimating Phase Velocity Using Arbitrarily Shaped Microtremor Arrays. In *Bulletin of the Seismological Society of America*, 92, 6, 2002

Oppo, D.: *Studio dei vulcani di fango per la definizione della migrazione dei fluidi profondi*. Università di Bologna, 2011

Parolai, S., Richwalski, S. M., Milkereit, C., & Fäh, D.: S-wave velocity profiles for earthquake engineering purposes for the Cologne area (Germany). In *Bulletin of Earthquake Engineering*, 4, 1, pp. 65–94. https://doi.org/10.1007/s10518-005-5758-2, 2006

Sciarra, A., Cantucci, B., Conventi, M., Ricci, T.: Caratterizzazione geochimica e monitoraggio dei flussi e delle componenti gassose nella Riserva delle Salse di Nirano, Atti della Società dei Naturalisti e Matematici di Modena – Supplemento, 148, 2017

Sciarra, A., Cantucci, B., Ricci, T., Tomonaga, Y., & Mazzini, A.: Geochemical characterization of the Nirano mud volcano, Italy. *Applied Geochemistry*, *102*, 77–87. https://doi.org/10.1016/j.apgeochem.2019.01.006, 2019

Sibiryakov, B., Leite, L. W. B., & Sibiriakov, E.: Porosity, specific surface area and permeability in porous media. *Journal of Applied Geophysics*, *186*. https://doi.org/10.1016/j.jappgeo.2021.104261, 2021

Socco, L. V., & Comina, C.: Time-average velocity estimation through surface-wave analysis: Part 2 - P-wave velocity. *Geophysics*, *82*(3), U61–U73. https://doi.org/10.1190/GEO2016-0368.1, 2017

Socco, L. V., Comina, C., & Anjom, F. K.: Time-average velocity estimation through surface-wave analysis: Part 1-s-wave velocity. *Geophysics*, *82*(3), U49–U59. https://doi.org/10.1190/GEO2016-0367.1, 2017

Tsai, C. C., & Asimaki, D.: Theoretical Vp prediction model for satured soil and rock. *Geotechnique Letters*. https://doi.org/80/jgele.25.00059, 2026

Tsai, C. C., Liu, H. W., & Asimaki, D.: Predicting Vp and constrained modulus reduction curve based on Vs and shear modulus reduction curve in accordance with poroelastic theory. *Geotechnique*, *73*(7), 636–647. https://doi.org/10.1680/jgeot.21.00143, 2023

Zheng, J., Zheng, L., Liu, H. H., & Ju, Y.: Relationships between permeability, porosity and effective stress for low-permeability sedimentary rock. *International Journal of Rock Mechanics and Mining Sciences*, *78*, 304–318. https://doi.org/10.1016/j.ijrmms.2015.04.025, 2015